J|A|C|S ARTICLES

Published on Web 09/10/2010

Density Functional Theory Calculations on the Mononuclear Non-Heme Iron Active Site of Hmd Hydrogenase: Role of the Internal Ligands in Tuning External Ligand Binding and Driving H_2 Heterolysis

Abhishek Dey*

Indian Association for the Cultivation of Science, 2A Raja S. C. Mullick Road, Kolkata, India 700032

Received May 23, 2010; E-mail: icad@iacs.res.in

Abstract: DFT calculations on active-site models of the non-heme Fe site of Hmd hydrogenase are reported. Binding of several biologically relevant ligands (e.g., CN^-, CO, H^-, H_2, and O_2) to the active site of Hmd was investigated using a method that reproduced the geometric and vibrational properties of the resting site. The results indicate that this neutral ferrous active site has higher affinity toward anionic ligands (e.g., H^- and CN^-) than π-acidic ligands (e.g., CO and O_2). Natural population analysis and molecular orbital analysis revealed that this is due to extensive delocalization of electron density into the low-lying unoccupied orbitals of the CO, acyl, and pyridinol ligands present in the active site. In addition to normal d$-\pi$ back-bonding, metal 3d orbital-mediated charge transfer from occupied ligand orbitals to the unoccupied orbitals of the internal ligands was observed. This charge transfer leads to systematic variations in the experimentally observed C$-$O stretching frequencies. Protonation of the thiolate ligand present in the active site significantly enhances these anion ligand binding affinities. In fact, the calculated vibrational frequencies indicate that CN^- binding is possibly associated with protonation of the thiolate ligand. The high affinity for binding of the anionic H^- ligand (where 81% of the electron density of H^- is delocalized into the active site) is calculated to play a dominating role in the H$-$H bond heterolysis step during catalysis. The binding energies of these ligands relative to the substrate, H_2, highlight the importance of a proposed structural reorganization during catalysis.

Introduction

Use of fossil fuel as the chief source of energy has added significant amounts of CO_2 to the atmosphere, which has led to several serious environmental issues. A H_2-based energy cycle has generated significant interest among researchers and entrepreneurs alike, as it should have minimal environmental impact. Commercially, H_2 can be produced by electrolysis of H_2O. However, affordable electrodes generally produce H_2 with a high overpotential.[1] In nature, H_2 is produced from water under ambient conditions without any overpotential in the active sites of enzymes called hydrogenases (H_2ases). There are three type of H_2ases. Iron-only and nickel$-$iron H_2ases are quite common in bacteria and contain multiple iron$-$sulfur clusters.[2−7] Very recently, a small archeal H_2ase that contains a single non-heme iron in its active site and no additional iron$-$sulfur sites has been isolated.[8−10] It catalyzes (Figure 1) the reversible dehydrogenation of methenyltetrahydromethanopterin (methenyl-H_4MPT) and hence is named H_2-forming methylenetetrahydromethanopterin dehydrogenase, or Hmd.

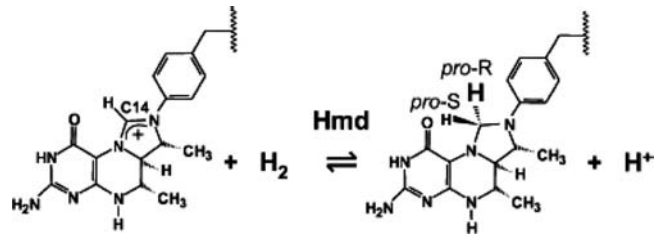

Figure 1. Reaction catalyzed by Hmd.

A recent crystal structure of Hmd has revealed that this enzyme has a mononuclear non-heme Fe in its active site (Figure 2 inset).[11,12] The Fe is ligated by two intrinsic CO molecules, a pyridinol nitrogen, an acyl anion bound via the acyl carbon, a thiolate ion, and a solvent molecule. This ligation description is consistent with EXAFS and FTIR data obtained for the active enzyme.[13,14] The N and acyl coordinations are derived from a

(1) Jones, A. K.; Sillery, E.; Albracht, S. P. J.; Armstrong, F. A. *Chem. Commun.* **2002**, 866–867.
(2) Armstrong, F. A.; Fontecilla-Camps, J. C. *Science* **2008**, *321*, 498–499.
(3) Armstrong, F. A.; Belsey, N. A.; Cracknell, J. A.; Goldet, G.; Parkin, A.; Reisner, E.; Vincent, K. A.; Wait, A. F. *Chem. Soc. Rev.* **2009**, *38*, 36–51.
(4) de Lacey, A. L.; Fernández, V. M.; Rousset, M. *Coord. Chem. Rev.* **2005**, *249*, 1596–1608.
(5) Fontecilla-Camps, J. C.; Volbeda, A.; Cavazza, C.; Nicolet, Y. *Chem. Rev.* **2007**, *107*, 4273–4303.
(6) De Lacey, A. L.; Fernandez, V. M.; Rousset, M.; Cammack, R. *Chem. Rev.* **2007**, *107*, 4304–4330.
(7) Lubitz, W.; Reijerse, E.; van Gastel, M. *Chem. Rev.* **2007**, *107*, 4331–4365.
(8) Shima, S.; Thauer, R. K. *Chem. Rec.* **2007**, *7*, 37–46.
(9) Hartmann, G. C.; Klein, A. R.; Linder, M.; Thauer, R. K. *Arch. Microbiol.* **1996**, *165*, 187–93.
(10) Buurman, G.; Shima, S.; Thauer, R. K. *FEBS Lett.* **2000**, *485*, 200–204.
(11) Shima, S.; Pilak, O.; Vogt, S.; Schick, M.; Stagni, M. S.; Meyer-Klaucke, W.; Warkentin, E.; Thauer, R. K.; Ermler, U. *Science* **2008**, *321*, 572–575.

10.1021/ja1041918

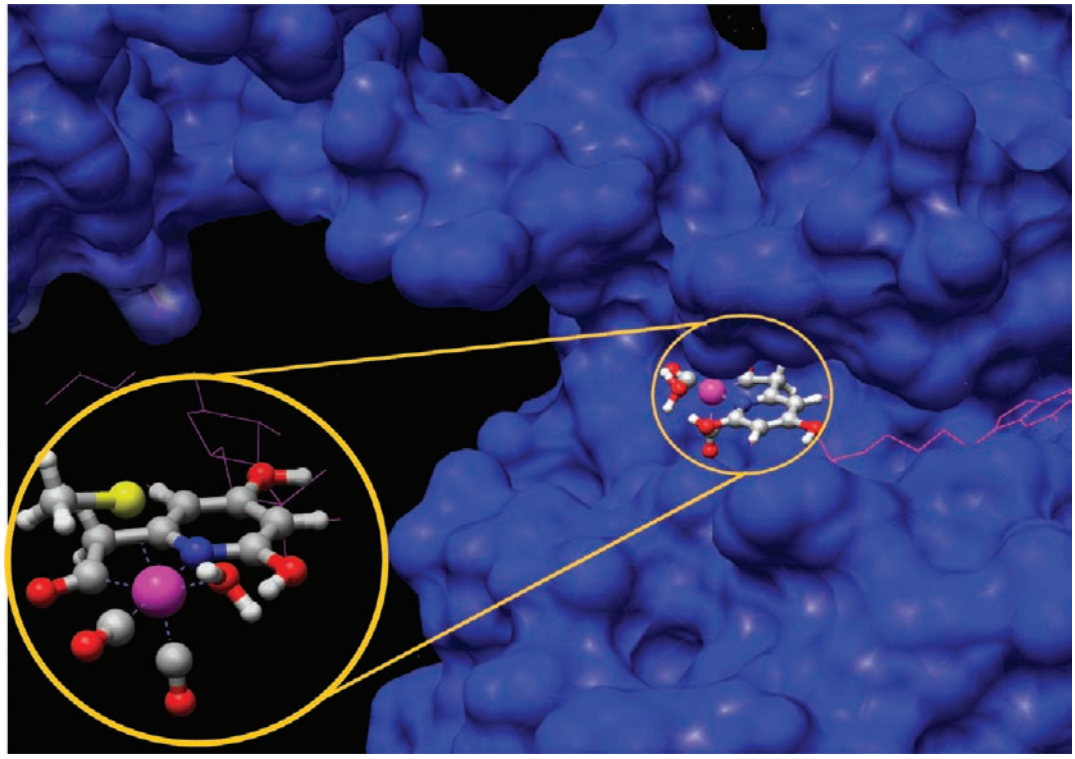

Figure 2. Solvent-exposed active site of Hmd H_2ase (PDB entry 3F46). The inset shows the DFT model of the active site used in this study. Fe, S, O, N, and C atoms are shown as pink, yellow, red, blue, and gray spheres, respectively.

guanylpyridinol cofactor. Additionally, in its native form, the active site sits on a solvent-exposed cleft of the enzyme (Figure 2).[12] Recent data indicate that the cosubstrate H_4MPT may cap this active site upon binding.[15] The electronic structure of Hmd has been investigated using FTIR spectroscopy, Mossbauer spectroscopy, and nuclear resonance vibrational spectroscopy (NRVS), and the data are consistent with a low-spin Fe(II) description of the active site.[14,16−18] Density functional theory (DFT) calculations are consistent with such interpretation,[19,20] and they have been further used to investigate the mechanism of H_2 reduction in significant detail.[21,22]

The enzyme does not bind its substrate, H_2, in the absence of the methenyl-H_4MPT cosubstrate.[14] External ligands such as CN^- and CO readily bind to the active site, replacing the exchangeable solvent-derived ligand.[14] This produces a dramatic effect on the FTIR and Mossbauer data obtained from the active site.[18] These exogenous ligands have been identified as inhibitors of Hmd, as they competitively bind to the Fe(II) center in the active site.[17] Interestingly, to inhibit the H_2ase activity of Hmd by 50%, ~100 μM CO is required, as opposed to ~1 and 20 μM CO required for Fe-only and Ni−Fe H_2ases, respectively.[8] Alternatively, Hmd H_2ase is inhibited by CN^- with a K_I of 0.2 mM, while the H_2ase activities of Fe-only and Ni−Fe H_2ases are not affected by the presence of CN^-.[8] This may imply that this Fe(II) site has a higher affinity for anionic ligands such as CN^- and a lower affinity for excellent π-acidic ligands such as CO relative to other hydrogenases. The enzyme is relatively stable and functional in O_2 in comparison with other H_2ases as well as other non-heme Fe(II) active sites with open coordination sites, as they generally rapidly react with O_2.[17,4,5]

In this work, the binding of Hmd with different types of ligands is investigated. On the basis of an analysis of the changes in electronic structure upon ligand binding, some of the unusual ligand-binding properties of the Hmd active site can be explained. In particular, the internal ligands of Hmd play a dominant role in tuning these properties via extensive charge delocalization. These properties have been found to dominate the H−H heterolysis process, and they also determine the relative affinities of CO and CN^- ligands.

Methods

All of the calculations were performed on the HPC cluster at IACS using the Gaussian 03 software package.[23] The geometries were optimized with the spin-unrestricted formalism using both the

(12) Hiromoto, T.; Ataka, K.; Pilak, O.; Vogt, S.; Stagni, M. S.; Meyer-Klaucke, W.; Warkentin, E.; Thauer, R. K.; Shima, S.; Ermler, U. *FEBS Lett.* **2009**, *583*, 585–590.
(13) Salomone-Stagni, M.; Vogt, S.; Shima, S.; Meyer-Klaucke, W. *J. Phys.: Conf. Ser.* **2009**, *190*, 012197.
(14) Lyon, E. J.; Shima, S.; Boecher, R.; Thauer, R. K.; Grevels, F.-W.; Bill, E.; Roseboom, W.; Albracht, S. P. J. *J. Am. Chem. Soc.* **2004**, *126*, 14239–14248.
(15) Hiromoto, T.; Warkentin, E.; Moll, J.; Ermler, U.; Shima, S. *Angew. Chem., Int. Ed.* **2009**, *48*, 6457–6460.
(16) Guo, Y.; Wang, H.; Xiao, Y.; Vogt, S.; Thauer, R. K.; Shima, S.; Volkers, P. I.; Rauchfuss, T. B.; Pelmenschikov, V.; Case, D. A.; Alp, E. E.; Sturhahn, W.; Yoda, Y.; Cramer, S. P. *Inorg. Chem.* **2008**, *47*, 3969–3977.
(17) Lyon, E. J.; Shima, S.; Buurman, G.; Chowdhuri, S.; Batschauer, A.; Steinbach, K.; Thauer, R. K. *Eur. J. Biochem.* **2004**, *271*, 195–204.
(18) Shima, S.; Lyon, E. J.; Thauer, R. K.; Mienert, B.; Bill, E. *J. Am. Chem. Soc.* **2005**, *127*, 10430–10435.
(19) Wang, X. F.; Li, Z. M.; Zeng, X. R.; Luo, Q. Y.; Evans, D. J.; Pickett, C. J.; Liu, X. M. *Chem. Commun.* **2008**, 3555–3557.
(20) Nakatani, N.; Nakao, Y.; Sato, H.; Sakaki, S. *Chem. Lett.* **2009**, *38*, 958–959.
(21) Yang, X.; Hall, M. B. *J. Am. Chem. Soc.* **2008**, *130*, 14036–14037.
(22) Yang, X.; Hall, M. B. *J. Am. Chem. Soc.* **2009**, *131*, 10901–10908.
(23) Frisch, M. J.; et al. *Gaussian 03*, revision C.02; Gaussian, Inc.: Wallingford, CT, 2004.

BP86[24,25] and B3LYP[26,27] functionals and the 6-311G* basis set. Frequency calculations were performed on each optimized structure using the same basis set to ensure that it was a minimum on the potential energy surface. The frequencies calculated using BP86 are reported as is, while the reported values calculated using the B3LYP functional were scaled by a factor of 0.95. Total energy calculations were performed using the 6-311+G* basis set and a convergence criterion of 10^{-10} hartree. Basis-set superposition error has been reported to be minimal (~1 kcal/mol) for anion binding at this level of theory.[28,29] A polarizable continuum model (PCM)[30] with an intermediate ε value of 11 was used to mimic the solvation of the partially solvent-exposed active site of Hmd. ΔG was obtained by adding the zero-point energy and the entropic contributions obtained with the mixed basis set used during optimization (either in the gas phase or after solvation correction) to the total energy. Although conventional solvation models work very well in describing protein active sites, they are often not sufficiently accurate in describing the solvation of small ions. Thus, experimental and/or theoretical *aqueous* solvation free energies (i.e., hydration energies) of the small ions investigated in this study were obtained from the literature.[31−33] The H−H heterolysis energy was calculated using the same computational techniques and aqueous solvation energies of the products. Except for the O_2-bound state, which has a triplet ground state, all of the other ligand-bound forms have singlet ground states.

Results

The Hmd active site was modeled (Figure 2 inset) using a 5-acyl-2-pyridinol ligand to represent the guanylpyridinol cofactor, a thiolate ligand to represent the axial cysteine, two CO molecules, and an exchangeable open coordination site that is occupied by H_2O in the native form. In some ferrous active sites, the cysteine ligand is proposed to be protonated.[34] The protonation state of the cysteine ligand could not be determined experimentally. Thus, this study considered both the deprotonated (thiolate, RS^-) and protonated (thiol, RSH) states of this ligand.

Choice of Ligands. The ligands chosen for these studies were H_2O (the resting site), CO and CN^- (known inhibitors of the H_2ase activity of Hmd),[17] H_2 (the substrate for Hmd), and H^- (the product of substrate heterolysis). In addition to these, the binding affinity of O_2 was investigated, as this site is one of the very few known curious cases of O_2-tolerant H_2ases.[35,36] N_3^- was used to investigate the binding of an innocent donor ligand. These exogeneous ligands interact with a transition metal quite differently: CO, CN^-, O_2, and H_2 can act as both donor and acceptor ligands because of the availability of filled donor orbitals and low-lying empty acceptor orbitals, whereas H^- is a σ donor and N_3^- can act as both a σ donor and a π donor.

Resting State. The geometries of the active site with different exchangeable ligands were optimized using the BP86 and B3LYP functionals. Experimentally, only the resting form has been characterized using high-resolution crystallography.[11] EXAFS data for the resting form are available, but the Fe−OH_2 bond length could not be unambiguously assigned on the basis of these data.[13] Comparison with the available structural data revealed that both the B3LYP and BP86 functionals reproduced the geometric parameters reasonably well (Table 1, experimental data in the first two rows). However, the optimized Fe−CO and C−O bond lengths calculated using the BP86 functional are in slightly better agreement with the experimental values.

The calculated vibrational frequencies for the CO ligands (Table 1, ν_{CO} column) were 1961 and 2012 cm^{-1} using BP86 and 1963 and 2007 cm^{-1} using B3LYP. Both of these sets of results match reasonably well with the experimentally observed CO stretches at 1944 and 2011 cm^{-1}.[14] It should be noted that a pyridonate tautomer (in which the pyridinol OH is deprotonated and the thiolate is protonated instead) was calculated to be 10 kcal/mol higher in energy, possibly as a result of the 19° rotation of the pyridine ring out of the equatorial plane in the optimized geometry, and thus, it was not considered in this study.

Upon protonation of the thiolate ligand, the Fe−S bond and the Fe−CO bonds elongate by 0.07 and 0.01−0.03 Å, respectively. Other than those, no other major structural distortions due to protonation of the thiolate ligand were observed.

The C−O stretches for the protonated (RSH) active-site model were calculated to be 2008 and 2048 cm^{-1} using B3LYP and 1994 and 2043 cm^{-1} using BP86. Both sets of values are much higher than the reported experimental values of 1944 and 2011 cm^{-1} for the resting state.

CO-Bound State. Exogenous CO is known to replace the H_2O ligand present in the resting active site.[14] Geometry optimizations indicate a stable exogenous-CO-bound structure. The Fe−C_{acyl} bond length was calculated to increase by 0.07−0.1 Å upon CO binding, depending on the functional used. The Fe−S bond is elongated by 0.05 Å, and the internal Fe−CO bonds are elongated by 0.01 Å. The Fe−CO bond length of the exogenous CO was calculated to be 1.85 Å using BP86 and 1.88 using B3LYP; these values are ~0.1 Å longer than those calculated for the internal CO ligands using the same functionals. Simultaneously, the C−O bond of the exogenous CO is shorter. It should be noted that the different Fe−CO bond lengths could not be determined on the basis of the EXAFS data, so an average bond length of 1.83 Å was reported.[37] These results indicate weaker bonding of the exogenous CO to the Fe site in comparison with the endogenous CO ligands, consistent with the experimental data.[14]

Solution FTIR data for the CO-bound state indicate three C−O vibrations at 1981, 2020, and 2074 cm^{-1}. Of these, the 2074 cm^{-1} peak has been identified as the external C−O stretch.[17] The C−O stretches were calculated as 1974, 1996, and 2052 cm^{-1} and 1983, 2008, and 2045 cm^{-1} using BP86 and B3LYP, respectively. These are in reasonable agreement with the experimental values.

(24) Becke, A. D. *Phys. Rev. A* **1988**, *38*, 3098–3100.
(25) Perdew, J. P. *Phys. Rev. B* **1986**, *33*, 8822–8824.
(26) Perdew, J. P.; Burke, K.; Ernzerhof, M. *Phys. Rev. Lett.* **1996**, *77*, 3865–3868.
(27) Becke, A. D. *J. Chem. Phys.* **1993**, *98*, 5648–5652.
(28) Gorelsky, S. I.; Basumallick, L.; Vura-Weis, J.; Sarangi, R.; Hodgson, K. O.; Hedman, B.; Fujisawa, K.; Solomon, E. I. *Inorg. Chem.* **2005**, *44*, 4947–4960.
(29) Rayon, V. M.; Valdes, H.; Diaz, N.; Suarez, D. *J. Chem. Theory Comput.* **2008**, *4*, 243–256.
(30) Miertus, S.; Scrocco, E.; Tomasi, J. *Chem. Phys.* **1981**, *55*, 117–129.
(31) Kelly, C. A.; Rosseinsky, D. R. *Phys. Chem. Chem. Phys.* **2001**, *3*, 2086–2090.
(32) Pliego, J. R.; Riveros, J. M. *Chem. Phys. Lett.* **2000**, *332*, 597–602.
(33) Wilhelm, E.; Battino, R.; Wilcock, R. J. *Chem. Rev.* **1977**, *77*, 219–262.
(34) Ogura, H.; Nishida, C. R.; Hoch, U. R.; Perera, R.; Dawson, J. H.; de Montellano, P. R. O. *Biochemistry* **2004**, *43*, 14712–14721.
(35) Goldet, G.; Wait, A. F.; Cracknell, J. A.; Vincent, K. A.; Ludwig, M.; Lenz, O.; Friedrich, B.; Armstrong, F. A. *J. Am. Chem. Soc.* **2008**, *130*, 11106–11113.
(36) Ludwig, M.; Cracknell, J. A.; Vincent, K. A.; Armstrong, F. A.; Lenz, O. *J. Biol. Chem.* **2009**, *284*, 465–477.
(37) Korbas, M.; Vogt, S.; Meyer-Klaucke, W.; Bill, E.; Lyon, E. J.; Thauer, R. K.; Shima, S. *J. Biol. Chem.* **2006**, *281*, 30804–30813.

Table 1. Experimental and Calculated Bond Lengths and Vibrational Frequencies (ν) of Hmd Active-Site Models (X is the Exchangeable Ligand)

method		bond lengths (Å)							ν (cm^{-1})	
		Fe−C_{acyl}	Fe−N	Fe−S	Fe−CO	Fe−X	C−O_{acyl}	C−O	ν_{CO}	ν_{intraX}
					X = H_2O					
exptl	Xtal[a]	1.91	2.01	2.38	1.86, 1.83	2.33	1.24	1.14	**1944**, **2011**[d]	
	EXAFS[b]	**1.88**	**2.05**	**2.33**	**1.76**			**1.17**		
B3LYP	RS^-	1.90	2.09	2.34	1.78, 1.78	2.36	1.21	1.14	1963, 2007	
	RSH	1.91	2.07	2.41	1.79, 1.81	2.39	1.20	1.14	2008, 2048	
BP86	RS^-	1.89	2.07	2.32	1.74, 1.76	2.42	1.21	1.16	1961, 2012	
	RSH	1.92	2.05	2.39	1.75, 1.76	2.42	1.21	1.15	1994, 2043	
					X = CO					
exptl	EXAFS[c]	**1.97**		**2.32**	**1.83**	**1.83**			**1981**, **2020**[d]	**2074**[d]
B3LYP	RS^-	1.97	2.09	2.39	1.79, 1.79	1.88	1.21	1.14	1983, 2008	2045
	RSH	2.01	2.09	2.42	1.82, 1.81	1.88	1.20	1.13	2033, 2046	2083
BP86	RS^-	2.01	2.06	2.37	1.75, 1.76	1.85	1.22	1.16	1974, 1996	2052
	RSH	2.03	2.07	2.39	1.78, 1.78	1.85	1.21	1.15	2011, 2043	2089
					X = CN^-					
exptl	EXAFS[c]	**2.00**		**2.34**	**1.79**	**1.97**			**1956**, **2020**[d]	**2091**[d]
B3LYP	RS^-	1.96	2.15	2.41	1.77, 1.77	1.99	1.22	1.15	2039, 2087	2194
	RSH	1.97	2.12	2.41	1.78, 1.79	1.98	1.21	1.14	1990, 2026	2102
BP86	RS^-	1.96	2.22	2.40	1.74, 1.75	1.97	1.22	1.17	1940, 1992	2086
	RSH	1.98	2.1	2.37	1.75, 1.75	1.96	1.22	1.16	1987, 2031	2101
					X = H^-					
B3LYP	RS^-	1.96	2.05	2.42	1.76, 1.76	1.62	1.22	1.16	1959, 2004	
	RSH	1.97	2.05	2.38	1.76, 1.77	1.60	1.21	1.14	1963, 2003	
BP86	RS^-	1.94	2.03	2.40	1.74, 1.74	1.64	1.23	1.17	1920, 1975	
	RSH	1.94	2.03	2.34	1.74, 1.74	1.61	1.22	1.16	1948, 1996	
					X = O_2					
B3LYP	RS^-	1.95	2.07	2.26	1.81, 1.81	2.07	1.20	1.14	2009, 2041	
	RSH	1.95	2.09	2.42	1.81, 1.82	2.19	1.13	1.13	2038, 2066	
BP86	RS^-	1.95	2.09	2.26	1.75, 1.79	2.06	1.21	1.16	1987, 2029	1202
	RSH	1.96	2.06	2.40	1.78, 1.78	2.01	1.20	1.15	2035, 2071	1276
					X = H_2					
B3LYP	RS^-	1.91	2.09	2.35	1.79, 1.78	1.78, 1.81	1.21	1.15	1974, 2023	
	RSH	1.94	2.06	2.42	1.80, 1.82	1.84, 1.88	1.20	1.13	1929, 2063	
BP86	RS^-	1.94	2.06	2.36	1.75, 1.76	1.78, 1.80	1.21	1.16	1973, 2025	
	RSH	1.95	2.05	2.39	1.77, 1.77	1.80, 1.85	1.21	1.15	2019, 2064	

[a] Crystal structure data for the resting state were taken from ref 11. [b] EXAFS data for the resting state were taken from ref 13. [c] EXAFS data for the CO- and CN^--bound sites were taken from ref 13. It should be noted that these data predate the recently published crystal structure. Thus, the presence of the bound acyl ligand was unforeseen during the EXAFS analysis, and a carboxylate ligand was assumed to be present instead. [d] Experimental vibrational frequencies were taken from ref 14.

Upon protonation of the thiol ligand, the major change in geometry is the elongation of the endogenous Fe−CO bonds by 0.03−0.02 Å and the Fe−C_{acyl} bonds by 0.02−0.04 Å, depending on the method used. There is also an elongation by 0.02 Å in the Fe−S bond and a shortening by 0.01 Å in the C−O_{acyl} bond.

The C−O vibrational frequencies upon protonation of the thiol were calculated as 2033, 2046, and 2083 cm^{-1} and 2011, 2043, and 2089 cm^{-1} using the B3LYP and BP86 functionals, respectively. These values are significantly higher than the experimental data reported for the CO-bound form.[14]

CN^--Bound State. CN^-, like CO, is known to bind to the open coordination site in Hmd.[17] The geometries computed using the two functionals show similar distortions upon CN^- binding. Relative to the resting-state geometry, the Fe−C_{acyl}, Fe−N, and Fe−S bonds were calculated to elongate by ∼0.06, ∼0.1, and ∼0.07 Å, respectively. Simultaneously, the Fe−CO bonds were shortened by 0.01 Å and the C−O bonds elongated by 0.01 Å. While the calculated Fe−CN bond length is in reasonable agreement with the experimental data, the calculated Fe−N bond and the Fe−S bond are significantly longer than the reported values.[37]

Solution FTIR data for the CN^--bound state indicate that the CN^- stretch is at 2091 cm^{-1} and that both of the CO stretches are shifted to higher values relative to the resting state, 1956 and 2020 cm^{-1}.[14] The DFT-calculated CN^- stretch using BP86 is 2086 cm^{-1}, which is in reasonable agreement with the experimental value. However, contrary to the experimentally observed shift to higher energy for the CO stretches upon CN^- binding (i.e., from 1944 and 2011 cm^{-1} to 1956 and 2020 cm^{-1}), the calculated values are significantly shifted toward lower energy (i.e., from 1961 and 2012 cm^{-1} to 1940 and 1992 cm^{-1}). The vibrational data obtained using B3LYP are 2039 and 2087 cm^{-1}, which are much higher than the reported experimental values.

Upon protonation, the major geometric changes calculated using the BP86 functional were elongation of the Fe−C_{acyl} bond by 0.02 Å, shortening of the Fe−N bond by 0.12 Å, and shortening of the Fe−S bond by 0.03 Å. The values and trends obtained using the B3LYP functional were mostly similar, except that no elongation of the Fe−S bond was observed. These geometric parameters, in particular the Fe−N and Fe−S bond lengths, are in much better agreement with the experimental EXAFS data[37] than those calculated for the deprotonated species.

The calculated CN stretch is 2101−2102 cm^{-1} using both methods, which is in reasonable agreement with the experimentally observed value of 2091 cm^{-1} (Table 1). The C−O

stretches obtained using the BP86 and B3LYP functionals are 1987 and 2031 cm^{-1} and 1990 and 2026 cm^{-1}, respectively. These values are in much better agreement with the experimental values than the values obtained for the active-site model with a deprotonated thiol. Notably, these CO stretches (1987 and 2031 cm^{-1} using BP86) are shifted to higher energies relative to those obtained for the resting state (1961 and 2012 cm^{-1} using BP86), as has been observed experimentally.[14]

In general, the geometric and vibrational parameters obtained using the BP86 functional are in better agreement with the experimental values. Thus, only the results obtained using the BP86 functional are discussed in the following sections, which concern models for which experimental values are not yet available. The corresponding values obtained using B3LYP are provided in Table 1.

H_2-Bound State. When the H_2O ligand was replaced with the substrate, H_2, no major change in the geometry of the active site was observed computationally. The H_2 is bound in a bidentate fashion, with the H−H axis parallel to the Fe−S bond.[22] The binding is asymmetric with one Fe−H bond slightly shorter than the other. The C−O stretches were calculated as 1973 and 2025 cm^{-1}, both of which are 10 cm^{-1} higher in energy than those calculated for the resting active site.

Protonation of the thiolate ligand leads to significant changes in the geometry of the active site, namely, elongation of the Fe−H_2 bond (by ∼0.03 Å), elongation of the Fe−S, Fe−C_{acyl}, and Fe−CO bonds, and shortening of the Fe−N bond. The elongation of the Fe−CO bonds is complemented by shortening of the C−O bonds, which leads to an increase in the C−O vibrational frequencies relative to those for the deprotonated active site. The calculated CO stretches are 2019 and 2064 cm^{-1} which are shifted to higher energy relative to those calculated for the deprotonated model.

H^--Bound State. Hydride results from the heterolytic splitting of the substrate H_2, and the H^--bound form of the active site is a proposed intermediate in the reaction cycle.[22] The H^- ligand forms a very short bond with the Fe^{II} center (Fe−H = 1.64 Å). Binding of H^- to the active site causes elongation of the trans Fe−C_{acyl} bond (by 0.05 Å) and the Fe−S bond (by 0.08 Å) relative to the resting state. One of the Fe−CO bonds is shortened by 0.02 Å (average), and the Fe−N bond is shortened by 0.04 Å. The C−O bonds were calculated to elongate by 0.02 Å. The weakening of the C−O bonds is also reflected in the calculated frequencies, which are lowered from 1961 and 2012 cm^{-1} in the resting state to 1920 and 1975 cm^{-1} in the H^--bound form.

Protonation of the H^--bound form leads to shortening of the Fe−S and Fe−H bonds. The C−O bonds are shortened by 0.01 Å, leading to strengthening of the C−O vibrations, which shift to higher energies of 1948 and 1996 cm^{-1} in the protonated form relative to 1920 and 1975 cm^{-1} in the deprotonated form.

O_2-Bound State. O_2 is known to bind to most Fe^{II} active sites in biological systems, including Fe-only and Ni−Fe hydrogenases. However, there are no reports of O_2 binding to Hmd. In fact, unlike most H_2ases, Hmd activity is not inhibited by the presence of O_2.[17] The DFT calculations predicted a stable O_2-bound structure. The Fe−S bond is significantly shorter (2.26 Å) relative to that in the resting state (2.32 Å), indicating a stronger Fe−S bond in the O_2-bound form. The Fe−C_{acyl} and Fe−CO are elongated by 0.06 and 0.02 Å (average), respectively. The C−O stretches are shifted to higher energies relative to the resting state upon O_2 binding.

The calculated CO stretches for the O_2-bound form are 1987 and 2029 cm^{-1}, which are significantly shifted to higher energies with respect to the H_2O-bound resting state. The O−O stretch was calculated as 1202 cm^{-1}, which is lower than that of molecular O_2 (calculated as 1538 cm^{-1}) and higher than that of O_2^- (calculated as 1113 cm^{-1}).

Upon protonation, the Fe−S bond is elongated by 0.14 Å and the Fe−O bond shortened by 0.05 Å; the Fe−CO bonds elongate, and the C−O bonds shorten. The calculated C−O stretches are 2035 and 2071 cm^{-1}, which are shifted to higher energies relative to those calculated for the deprotonated O_2-bound state. The O−O stretch is also shifted to a higher energy of 1276 cm^{-1} relative to the value of 1202 cm^{-1} calculated for the deprotonated O_2-bound model.

Nature of the Bonding. The electronic configuration of the Fe active site is best described as $t_2^6e^0$ (i.e. low-spin Fe^{II}). Because of extensive mixing of the Fe d orbitals with the ligand orbitals, a density of states (DOS) diagram is a more convenient way to represent its electronic structure than a molecular orbital diagram. The DOS for the resting state (Figure 3A) shows the occupied t_2 orbitals below 0 eV (the HOMO energy was set to 0 eV). In addition to the empty set of e orbitals (blue bars between 0−3 eV), there is significant d-orbital mixing (blue bars above 3.3 eV) into the CO π^* (Figure 3A red bars and Figure 3B), pyridinol π^* (Figure 3A green bars), and acyl π^* (Figure 3A pink bars and Figure 3C) orbitals. These are mainly the t_2 orbitals on the metal, and they provide a way to transfer electron density away from the metal center into these π-acceptor ligands. In addition to direct charge transfer from the occupied orbitals of the metal to the unoccupied orbitals of the π-acceptor ligands, the t_2 orbitals also provide a pathway for charge transfer from occupied ligand orbitals to these unoccupied ligand π^* orbitals. This is clear from the contour of the occupied S 3p donor orbital (Figure 3D), where CO π^* mixing is observed. This arises because the metal t_2 orbital that overlaps with the S 3p orbital also overlaps with the CO π^* orbital, providing mechanism for a metal t_2 orbital-mediated charge transfer from the occupied S 3p orbital to the unoccupied CO π^* orbital. This provides a ligand-to-ligand charge-transfer pathway that allows efficient charge delocalization within the Hmd active site.

The presence of extensive back-bonding interactions between the Fe and the π-acceptor ligands present leads to efficient delocalization of the charge of a bound ligand. The electrostatic potential plots (Figure 4) show that when anionic ligands such as H^- are bound (Figure 4B), the electron densities on the CO, acyl, thiol, and pyridinol units become more negative. Alternatively, binding an electron-density-withdrawing ligand such as CO (Figure 4C) or O_2 (Figure 4D) leads to depletion of electron density from these units. Table 2 indicates the differences in natural population analysis (NPA) charge on relevant centers of the different ligand-bound forms relative to the resting state. For anionic ligands such as N_3^-, CN^-, and H^-, the NPA charges on the bound ligands indicate a significant reduction in the charge density relative to the free anions (indicated by positive values in the X column). For example, the calculated NPA charge on the H atom of a bound H^- ligand is −0.19 (Table 2), which means that ∼81% of the negative charge of the H^- ligand is delocalized off the initial H^- center. The differences in NPA charges indicate that only a part of this charge (−0.156) is delocalized onto the Fe center. The rest of it is delocalized into the acyl group (−0.191), the CO groups (−0.102), and the pyridinol group (−0.206), as indicated by

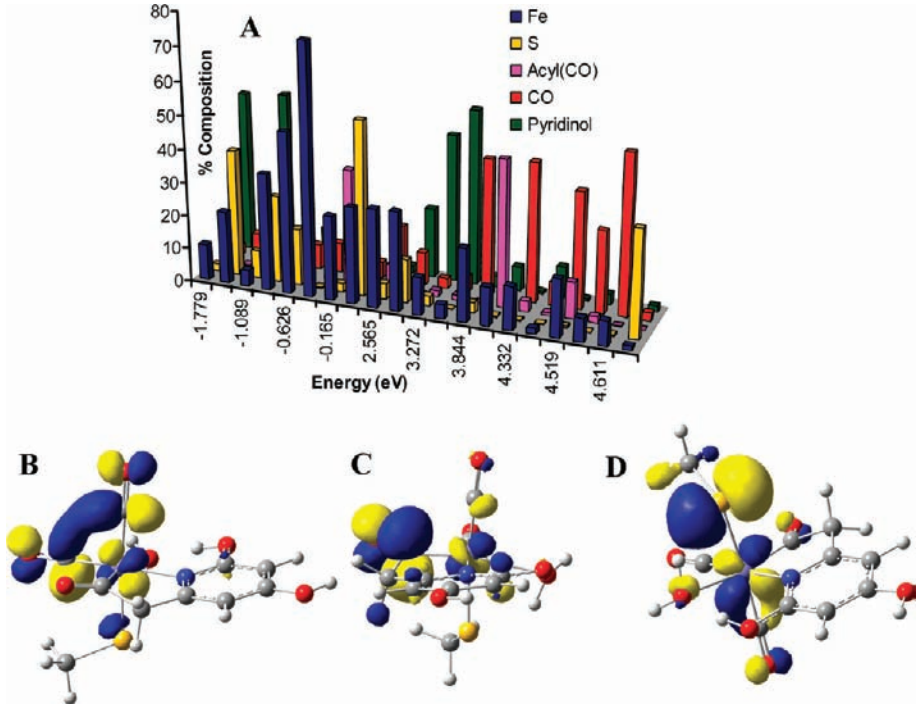

Figure 3. (A) DOS of the resting state, where the contributions of the individual fragments into the molecular orbitals are indicated by the histogram heights. (B) One of the four CO π^* orbitals showing back-bonding from occupied t_2 orbitals on Fe. (C) Acyl C−O π^* orbital showing a significant back-bonding interaction with one of the occupied t_2 orbitals. (D) S 3p donor orbital.

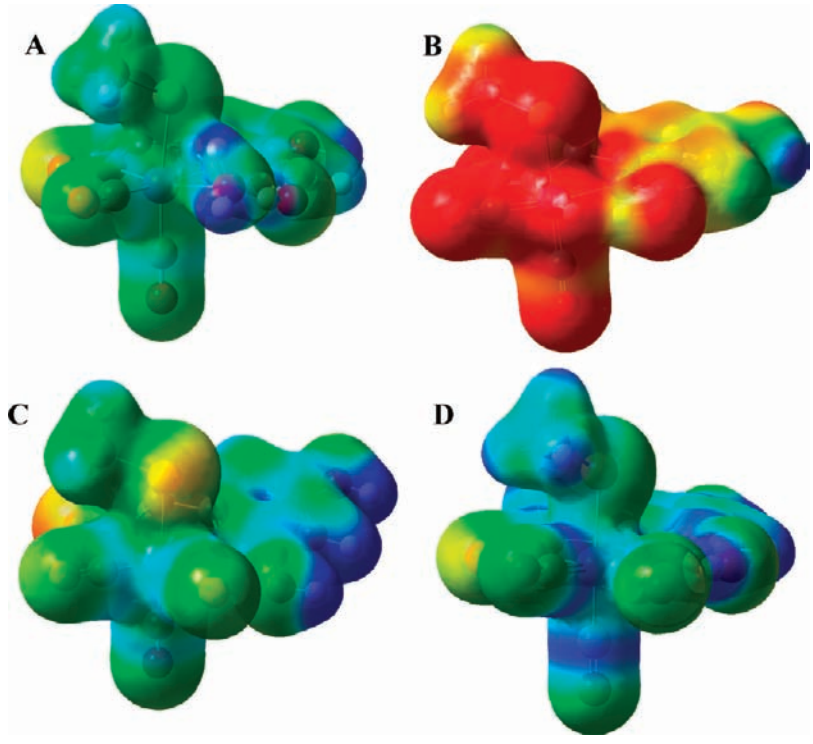

Figure 4. Electrostatic potential plots of (A) resting, (B) H^--bound, (C) CO-bound, and (D) O_2-bound states of Hmd H_2ase. The electron density gradient is given by red > yellow > green > blue.

the increase in negative charge density on these ligands (Figure 4B). This delocalization of charge density from an anionic ligand into the auxiliary ligands of the active site stabilizes the binding of the anionic ligand to this Fe^{II} center. This increase in charge density of the CO ligands leads to population of its unoccupied antibonding orbitals, resulting in weakening of the C−O bonds and a decrease in the C−O frequencies upon anionic ligand binding to the Fe center, as was observed above (e.g., H^- acting as a donor ligand leads to lower C−O vibrational frequencies).

π-Acceptor ligands such as CO and O_2 withdraw electron density from the active site, as indicated by the corresponding negative values in the X column in Table 2, the increased electron densities on these ligands, and the decreased charge densities on the thiol and CO supporting ligands after binding

Table 2. Calculated Changes in NPA Charges Relative to the Resting State

	change in NPA charge					
ligand X	Fe	CO_{acyl}	CO	S	pyridinol	X
CO	−0.151	−0.152	0.076	0.113	0.116	−0.036
CN^-	−0.110	−0.164	−0.011	−0.071	−0.025	0.419
N_3^-	0.003	−0.129	−0.041	−0.017	−0.203	0.424
H^-	−0.156	−0.191	−0.102	−0.116	−0.206	0.808
O_2	0.147	−0.067	0.134	0.248	0.046	−0.470
H_2	−0.165	−0.044	0.021	0.063	0.042	0.121

Table 3. Calculated ΔG (kcal/mol) for Ligand Binding to the Deprotonated Active Site

	gas-phase		PCM ($\varepsilon = 11.0$)		active-site PCM + aq. solvation	
ligand	B3LYP	BP86	B3LYP	BP86	B3LYP	BP86
CO	7.05	−0.81	−3.73	−5.38	−5.85	−9.65
CN^-	−32.98	−36.18	−7.84	−15.37	4.04	−2.68
N_3^-	−26.12	−27.76	−2.03	−3.83	15.06	11.62
H^-	−79.57	−77.20	−39.39	−41.83	−18.07	−18.02
O_2	15.48	8.98	12.70	5.39	12.18	1.36
H_2	22.74	20.99	21.70	19.99	19.71	15.8

(Figure 4C,D). While this effect is smaller for CO, it is significant for O_2. Depletion of the electron density of the auxiliary ligands (thiol, 0.248; CO, 0.134) compensates for the increase in electron density on O_2. This charge transfer from the thiolate ligand leads to a very short Fe−S bond (2.26 Å), while the charge transfer from the internal CO ligands shifts the C−O vibrations to higher energies (from 1961 and 2012 cm^{-1} to 1987 and 2029 cm^{-1}).

H_2 binding leads to depletion of charge density from H_2, indicating that it acts as a donor ligand. The donated charge from H_2 is mostly localized on the Fe center.

Interestingly, the negative charge density on the acyl ligand increases in all of the above cases, where the weakly bound water has been displaced by a better donor ligand. Thus, this increase in total negative charge density on the aryl unit reflects the trans effects of these ligands. On the basis of the negative charge density on the acyl group, these ligands can be arranged in increasing order of their trans effect as follows: $H_2O < H_2 < O_2 < N_3^- < CO < CN^- < H^-$.

Binding Energies. The free energies (ΔG) of ligand binding to the deprotonated active site are listed in Table 3. Since the protein active site is partially solvent-exposed, the total energies were calculated using a full PCM in which both the active site and the small-molecule fragments were embedded in a medium with $\varepsilon = 11$ as well as a model in which the active sites were embedded in a PCM with $\varepsilon = 11$ and the experimental solvation energies of the small molecules were used. The later model accounts for the additional stabilization of the anions by hydrogen bonding in the aqueous solvent.

In general, BP86 predicted higher binding energies than B3LYP (Table 3). The binding energies of anions were overestimated in the gas phase. Upon inclusion of the solvation correction, a significant reduction in binding energy occurred. The reduction was maximum when experimental solvation energies were used, as inclusion of the hydrogen bonding of the free anions stabilized the reactants. CO binding to the active site was calculated to be energetically favorable after solvation correction (Table 3, row 1), consistent with the experimentally observed CO binding to the active site.[14] The binding energies of H_2 and O_2 to the Hmd active site are unfavorable (Table 3, rows 5 and 6), consistent with the experimental data.[17]

Table 4. Calculated ΔG (kcal/mol) for Ligand Binding to the Protonated Active Site

	PCM ($\varepsilon = 11.0$)		active-site PCM + aq. solvation	
ligand	B3LYP	BP86	B3LYP	BP86
CO	0.13	−4.49	0.23	8.98
CN^-	−26.40	−33.17	−14.52	−20.48
N_3^-	−24.81	−30.07	−7.728	−17.71
H^-	−63.54	−63.84	−42.22	−45.82
O_2	15.59	13.48	15.08	9.45
H_2	13.96	16.45	11.96	12.26

Anionic ligands were calculated to have favorable binding energies to the neutral Fe^{II} site of Hmd. In the gas phase and after inclusion of the PCM solvation correction, the anions were calculated to have stronger binding affinities than the π-acidic ligands CO and O_2. Experimentally, only CN^- is known to bind the Fe center of Hmd, and H^- has been proposed to stay bound to the Fe after H−H bond cleavage.[18,22] However, the calculations did not provide unambiguous evidence that binding of CN^- to the deprotonated Fe active site is thermodynamically feasible. In fact, when the experimental solvation energies of small molecules were used, B3LYP predicted an unfavorable ΔG for CN^- binding (Table 3, row 2), which is inconsistent with the experimental results. H^- has a calculated binding energy of −18 kcal/mol (Table 3, row 4), which is higher than those of all the other ligands tested. The innocent anionic donor ligand N_3^- did not have a very favorable energy for binding to the deprotonated resting active site when experimental solvation energies were used (Table 3, row 3).

The binding energies changed significantly when the thiolate ligand in the active site was protonated (Table 4). The binding energies of the anionic ligands [i.e., CN^-, N_3^-, and H^- (Table 4, rows 2−4) were significantly enhanced because of the increased positive charge on the active site. Alternatively, the affinity of the π-acidic ligands, such as CO, was significantly reduced when the thiolate was protonated. This is the case because the protonated active site has reduced electron density and hence does not have a significant back-bonding interaction with the π-accepting orbitals on CO. This produces an interesting effect on the relative binding affinities of O_2 and H_2. In the deprotonated active site, O_2 binding was significantly favored (7−12 kcal/mol more favorable; Table 4, rows 5 and 6) over H_2 binding, whereas in the protonated active site, the H_2 binding affinity is comparable to that of O_2 (lower in the case of B3LYP). This is primarily because of the differences in the nature of the bonding to the active site by these ligands. While H_2 acts as a donor ligand, O_2 acts as a π-acceptor ligand. Thus, protonation enhances H_2 binding and weakens O_2 binding.

Discussion

Lewis Acidity of a Neutral Fe^{II} Center. In general, Fe^{II} centers in neutral active sites are weak Lewis acids, and they show very weak affinities toward anion binding. In contrast, binding affinities of π-acidic ligands are strong. The active site in Hmd is neutral and has the iron in a formal Fe^{II} state. However, this site shows significant binding affinity toward anionic ligands such as CN^- and H^-. This is because the negative charge density of these ligands is delocalized onto the internal CO and the pyridinol ligands. These ligands have empty, low-lying unoccupied orbitals that participate in extensive back-bonding interactions with the occupied Fe d orbitals. Additionally the electron density of the bound anionic ligand is efficiently delocalized into the π^* orbitals of the internal CO and pyridinol

ligands. This charge-transfer process is allowed by the presence of d orbitals on Fe that interact simultaneously with both the donor orbitals of the bound anionic ligands and the acceptor orbitals of the internal ligands, The t_2^6 metal center therefore acts as a pathway for charge transfer from occupied ligand donor orbitals to unoccupied ligand π^* orbitals. Thus, a combination of the direct d$-\pi$ back-bonding and metal-mediated charge-transfer processes makes this active site a potent Lewis acid in spite of the fact that it has a neutral, formally Fe^{II} active site.

Spectator CO Vibrations. The CO vibrations of the internal CO ligands present in the active site provide insight into the nature of the ligand binding. Binding of donor ligands leads to lowering of the CO vibrational frequencies, as electron density is delocalized from these ligands into the CO π^* orbitals as a result of the presence of efficient metal-mediated pathways for ligand-to-ligand charge transfer. This effect is most dramatic for anionic ligands such as H^-, CN^-, and N_3^- where the average CO vibrations are shifted by 39, 21, and 29 cm^{-1}, respectively. π-Accepting ligands such as O_2, on the other hand, compete for d$-\pi$ back-bonding, leading to depopulation of the CO π^* orbitals and shifting the C$-$O vibrations higher by 22 cm^{-1}. Thus, these ligands can be arranged in order of increasing C$-$O vibrational frequency as follows: $H^- < N_3^- < CN^- < CO = H_2O < H_2 < O_2$. Here H^- produces the maximum population in the CO π^* orbitals and the lowest C$-$O vibrational frequencies, while O_2 produces the minimum population in the CO π^* orbitals and the highest C$-$O vibrational frequecies.

The CO vibration of the internal acyl CO bond also varies depending on the trans ligand. On the basis of the shifts in the $C-O_{acyl}$ stretching frequencies, the ligands can be arranged in order of increasing $C-O_{acyl}$ vibrational frequency as follows: $H^- < N_3^- < CN^- < CO < H_2 < O_2 = H_2O$. The C$-$O vibrations of the C$=$O unit of this group reflects the extent of back bonding into its π^* orbital. Thus this series, like the one above, reflects decreasing order of back-bonding into the acyl CO π^* orbital.

Protonation-Coupled Ligand Binding. The Hmd active site with a protonated thiolate ligand has a much higher affinity for binding donor ligands. Thus, CN^-, N_3^-, and H^- are all predicted to bind to the protonated active site. However, the protonation energy must be taken into account in order to get the total energy of this protonation-coupled ligand-binding step.

Protonation-coupled ligand binding involves two steps, as represented below:

$$Fe-Hmd-H_2O + H^+ \rightleftarrows Fe-HHmd-H_2O \quad (1)$$

$$Fe-HHmd-H_2O + X \rightleftarrows Fe-HmdH-X + H_2O \quad (2)$$

Here, reaction 1 represents protonation of the resting state, ΔG for which is the proton affinity of the resting state; reaction 2 represents the binding of the exchangeable ligand to the protonated active site. The sum of the free energies for these two steps represents the total free energy of protonation-coupled ligand binding ($\Delta G_{H^+,X}$).

When the proton affinity of the resting state (8.3 kcal/mol) is taken into account, all of the anionic ligands in general show favorable protonation-coupled binding to the active site (Table 5). π-Acceptor ligands such as CO and O_2 show weaker binding affinities to the protonated active site than to the deprotonated site (Table 5). This is due to the reduction of charge density on the active site as a result of protonation. While this makes the protonated active site a better electron acceptor (stronger binding with anionic ligands), it also makes it a weaker electron donor (weaker binding to π-acceptor ligands).

Table 5. Calculated Free Energy of Protonation-Coupled Ligand Binding Relative to the Resting State

	$\Delta G_{H^+,X}$ (kcal/mol)	
ligand	BP86	B3LYP
H_2O	0	0
O_2	17.58	21.08
CO	−0.62	6.23
H_2	20.39	17.96
CN^-	−12.35	−8.52
H^-	−37.69	−36.22
N_3^-	−9.57	−1.73

The calculated geometric parameters, C$-$O vibrational frequencies, and $\Delta G_{H^+,X}$ values combine to suggest the following:

(1) The resting form is deprotonated [better agreement with the geometry and with the calculated CO frequencies of the deprotonated form (those of protonated form are too high); unfavorable proton affinity].

(2) The CO-bound form is deprotonated [$\Delta G_{H^+,X}$ is not definitive, but the calculated C$-$O frequencies of the deprotonated form are in much better agreement with the measured CO frequencies (those of the protonated form are too high)].

(3) The CN^--bound form is protonated [better agreement with geometry (Fe$-$S, Fe$-$N are too long in the deprotonated form) and with the CO frequencies (those of the deprotonated form are too low); very favorable $\Delta G_{H^+,X}$].

(4) The H^--bound form should also be protonated, as proposed by Yang and Hall.[22]

Recently, a synthetic model complex of the Hmd active site containing thiolate, acyl, and phosphine ligands was reported.[38] The vibrational frequencies of the CN^--bound form of this complex, in which the thiolate ligand is deprotonated, are 1954 and 2012 cm^{-1} for C$-$O and 2050 cm^{-1} for C$-$N, which are similar to those reported for the enzyme (1956 and 2020 cm^{-1} for C$-$O and 2090 cm^{-1} for C$-$N). DFT calculations on this model with the BP86 functional gave vibrational frequencies of 1959 and 2005 cm^{-1} for C$-$O and 2110 cm^{-1} for C$-$N, which are in good agreement with the reported experimental values.[38] This indicates that the extent of back-bonding into the CO π^* orbitals, which determines the C$-$O vibrational frequencies, is similar in the thiolate-bound model complex and the thiol-bound active-site model. This is the case because the weaker donation by the phosphine ligand in the model complex relative to the nitrogen donor in the active site compensates for the strong donation of the thiolate ligand in the model complex relative to the thiol ligand at the active site.

Heterolytic H$-$H Bond Splitting. H$-$H bond heterolysis is calculated to be endothermic by 44 kcal/mol. However, in the active site of Hmd, after the initial binding of H_2, the H$-$H bond heterolysis is *exothermic* by 11.1 kcal/mol (Scheme 1, bottom). Since the two products of H_2 heterolysis (i.e., H^+ and H^-) possibly stay bound to the active site after cleavage (H^- bound to Fe and H^+ protonating the thiolate),[22] their interaction energy must provide the energy required for H$-$H bond heterolysis. To evaluate the individual contributions from binding of H^- to the active site and protonation of the thiolate, an alternate cycle in which the components of a heterolytically

(38) Royer, A. M.; Rauchfuss, T. B.; Gray, D. L. *Organometallics* **2009**, *28*, 3618–3620.

Scheme 1. Energy Decomposition of H_2 Heterolysis

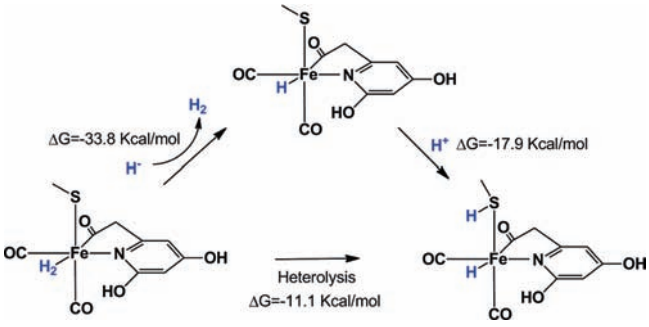

Scheme 2. Relative Energies of the H^--Bound Active Site with (left) and without (right) Dihydrogen Bonding

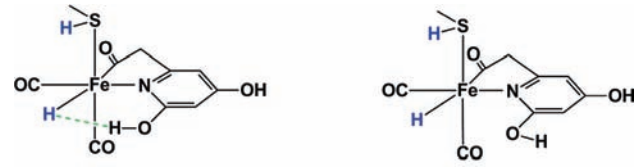

split H_2 molecule (i.e., a H^- anion and a H^+ cation) separately interact with the active site was constructed. The H^--binding step, in which H^- replaces the bound H_2, is exothermic by 33.8 kcal/mol (Scheme 1, top), and the protonation step is exothermic by 17.9 kcal/mol. Thus, the binding of H^- to the active site provides the major driving force required for H−H heterolytic splitting (calculated to be 44 kcal/mol with consideration of aqueous solvation). DFT calculations showed that once this H^- is bound to Fe, it can be efficiently transferred to the substrate.[22] As discussed earlier, such exothermic H^- binding is an unusual property of this neutral active site and is due to the efficient delocalization of the anionic charge into the π-acceptor ligands.

There is a direct dihydrogen bonding interaction between the bound H^- and the OH group at the 2 position of the pyridinol ligand (Scheme 2). The H···H distance was calculated to be 1.36 Å (BP86), which is ideal for a dihydrogen bond. Yang and Hall[22] have observed this dihydrogen bond and proposed that this may play a significant role in catalysis. To evaluate the energy of this dihydrogen bond, the relative energies of two geometries of the product of the H_2 heterolysis (Scheme 2) were calculated; in one of the structures, the OH group is rotated 180° to avoid formation of the dihydrogen bond. Their relative energies indicate that the energy of this dihydrogen bond is 8 kcal/mol, which is significant and directly adds to the favorable ΔG for H^- binding to the Fe.[39,40]

Inhibitor Binding to Hmd. CO and CN^- are known inhibitors of Hmd. O_2 is a known inhibitor of other H_2ases.[17] Binding of CO or CN^- was calculated to be energetically favorable relative to the substrate, H_2, irrespective of the method and the solvation model used. Although binding of O_2 to resting state of Hmd is calculated to be energetically unfavorable, it is again more favorable than binding of H_2. This implies that Hmd should bind these inhibitors preferentially over its substrate H_2. However, Hmd is not inhibited by O_2, and high concentrations of CO (an order of magnitude more than Fe-only H_2ases) and CN^- are required for inhibition of Hmd, in spite of their favorable binding energies. It is likely that binding of the substrate H_4MPT can significantly alter this. Although the crystal structure of H_4MPT-bound Hmd shows the H_4MPT to be bound 9.3 Å away from the active site, a recent study has suggested that during turnover, as a result of a large conformational change, H_4MPT possibly caps the Hmd active site, giving a distance of only ∼3 Å between the Fe and the reactive carbon center of H_4MPT.[15] Such a small cavity would not be large enough to accommodate H_2O (in the resting form), CO, CN^-, or O_2 but would be sufficient to fit the side-on-bound H_2. To evaluate this possibility, space-filling models of the active site with the H_4MPT cofactor bound near the active site were constructed (Figure 5). The distance between the Fe and the reactive carbon center of H_4MPT was fixed at ∼4.5 Å on the

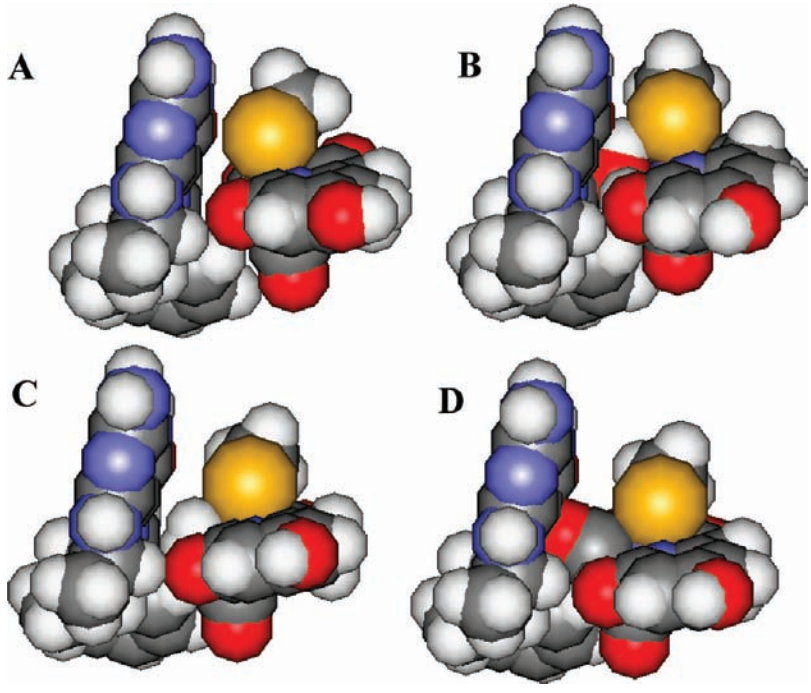

Figure 5. Hypothetical space-filling models of the H_4MPT-bound Hmd active site in which H_4MPT has been fit next to the optimized geometry of the active site (A) without any ligand, (B) with bound H_2O, (C) with H_2, and (D) with CO.

basis of the optimized geometries of Yang and Hall.[22] These models clearly show that the cavity between the H_4MPT and the Hmd active site is sufficiently large to bind H_2 (Figure 5C) but too small for binding of a H_2O (Figure 5B) or CO (Figure 5D) molecule, as such binding would result in significant van der Waals repulsion. Thus, H_2O, CO, and CN^- bind Hmd in its resting state as a result of their favorable binding energies, but their binding must be significantly destabilized during turnover because of steric constraints imposed by the capping of the active site by the cosubstrate as a result of the conformational change, thereby accounting for their weak inhibition of the H_2ase activity of Hmd.

The free energy of H_2 binding to the active site has been found to be unfavorable in this study and previous studies.[22] This is consistent with experimental results that also show no H_2 binding to the Hmd active site in absence of H_4MPT.[14] It must be emphasized that this binding energy represents the displacement of the bound H_2O ligand in the resting state by H_2. Thus, H_2O acts as an inhibitor of Hmd as it competes with its substrate for binding to the active site. The space-filling model of the resting site in the presence of H_4MPT (Figure 5B) suggests that the bound H_2O would not fit into the cavity and would possibly dissociate on H_4MPT binding, resulting in subsequent H_2 binding affinity of this active site.

Acknowledgment. The author acknowledges the IACS startup grant.

Supporting Information Available: Complete ref 23 and optimized geometries. This material is available free of charge via the Internet at http://pubs.acs.org.

JA1041918

(39) Szymczak, N. K.; Tyler, D. R. *Coord. Chem. Rev.* **2008**, *252*, 212–230.
(40) Kubas, G. J. *Chem. Rev.* **2007**, *107*, 4152–4205.